Cell

Simian Virus 40 Depends on ER Protein Folding and Quality Control Factors for Entry into Host Cells

Mario Schelhaas,[1] Johan Malmström,[2] Lucas Pelkmans,[2] Johannes Haugstetter,[1] Lars Ellgaard,[1,3] Kay Grünewald,[4] and Ari Helenius[1,*]
[1]Institute of Biochemistry and
[2]Institute of Molecular Systems Biology
Schafmattstrasse 18, ETH Hoenggerberg, ETH Zurich, CH-8093 Zurich, Switzerland
[3]Department of Molecular Biology, Universitetsparken 13, University of Copenhagen, DK-2100 Copenhagen, Denmark
[4]Department of Molecular Structural Biology, Max-Planck-Institute of Biochemistry, Am Klopferspitz 18, D-82152 Martinsried, Germany
*Correspondence: ari.helenius@bc.biol.ethz.ch
DOI 10.1016/j.cell.2007.09.038

SUMMARY

Cell entry of Simian Virus 40 (SV40) involves caveolar/lipid raft-mediated endocytosis, vesicular transport to the endoplasmic reticulum (ER), translocation into the cytosol, and import into the nucleus. We analyzed the effects of ER-associated processes and factors on infection and on isolated viruses and found that SV40 makes use of the thiol-disulfide oxidoreductases, ERp57 and PDI, as well as the retrotranslocation proteins Derlin-1 and Sel1L. ERp57 isomerizes specific interchain disulfides connecting the major capsid protein, VP1, to a crosslinked network of neighbors, thus uncoupling about 12 of 72 VP1 pentamers. Cryo-electron tomography indicated that loss of interchain disulfides coupled with calcium depletion induces selective dissociation of the 12 vertex pentamers, a step likely to mimic uncoating of the virus in the cytosol. Thus, the virus utilizes the protein folding machinery for initial uncoating before exploiting the ER-associated degradation machinery presumably to escape from the ER lumen into the cytosol.

INTRODUCTION

During entry into host cells, animal viruses typically undergo a process of stepwise destabilization and uncoating according to a program that is linked in time and space with the movement of the particle from compartment to compartment in the cell (Marsh and Helenius, 2006).

In this study, we have analyzed the uncoating and penetration of Simian virus 40 (SV40), a simple, nonenveloped DNA virus of the polyoma virus family. It uses the ganglioside GM1 as receptor, and enters host cells by activating the caveolar/lipid raft pathway of endocytosis (Damm et al., 2005; Pelkmans et al., 2001; Tsai et al., 2003). After internalization, the first station is the caveosome, a pH-neutral, caveolin-containing endocytic organelle distinct from classical endosomes. From the caveosome, the virus moves in noncaveolar vesicles along microtubules to the endoplasmic reticulum (ER) (Kartenbeck et al., 1989; Pelkmans et al., 2001). After translocation from the ER into the cytosol, the virus is thought to enter the nucleus via nuclear pore complexes where transcription and replication take place (Clever et al., 1991; Estes et al., 1971; Nakanishi et al., 1996).

SV40 and related polyoma viruses are unusual in several respects. First, their DNA genome is associated with histones in a circular complex containing 20–22 nucleosomes (Varshavsky et al., 1977). Second, the 50 nm capsids are composed of homopentamers of the major capsid protein, VP1 (43 kDa) associated with one of the minor structural proteins VP2 or VP3. The virus has icosahedral (T = 7) symmetry, and contains 72 pentamers of which 12 are five- and 60 six-coordinated (Liddington et al., 1991). The pentamers are connected to each other via C-terminal peptides extending from a VP1 molecule in one pentamer to docking sites present in two VP1 molecules of a neighboring pentamer stabilized by calcium ions (Ca^{2+}) (Li et al., 2003). The pentamers are linked to each other by disulfide bonds between cysteine 104 (C104) residues (Liddington et al., 1991).

The aim of our study was to determine why SV40 uses such an unusual and elaborate entry pathway and to define possible roles for the ER in the entry process. We found that isomerization of interpentamer disulfide bonds in the virus particle plays a central role in the uncoating process. To initiate disassembly, the virus takes advantage of the protein folding and quality control machinery present in the ER, before exploiting components of the ER-associated degradation (ERAD) presumably to escape from the ER lumen to the cytosol.

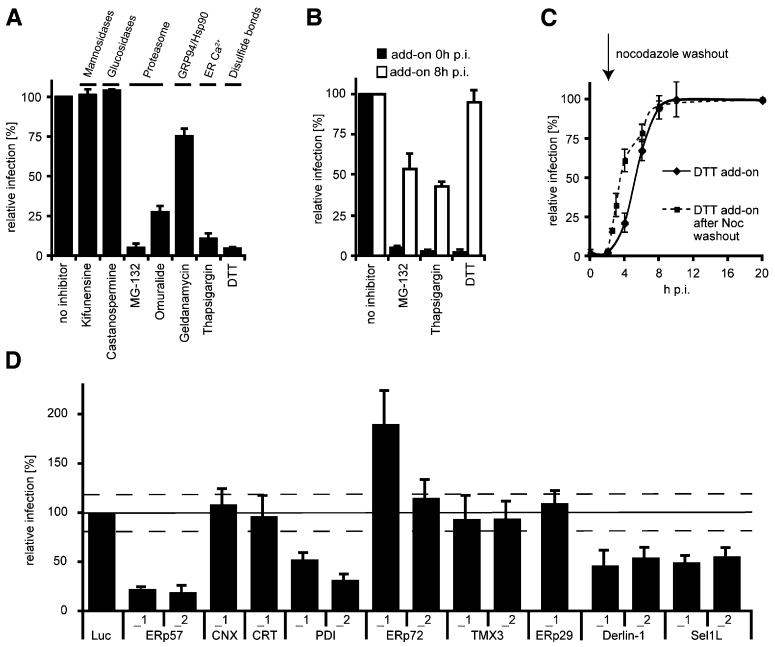

Figure 1. ER Processes and ER Proteins Are Associated with SV40 Infection

CV-1 (A–C) or HeLa (D) cells were infected with SV40 (one plaque-forming unit (PFU)/cell). The data represent the average ± SD of three independent experiments.

(A) Pharmacological inhibitors were added 30 min prior to addition of virus and present during infection (100 μM kifunensine, 5 μM castanospermine, 20 μM MG-132, 5 μM omuralide, 2 μM geldanamycin, 1 μM thapsigargin, and 5 mM DTT).

(B) As in (A). Inhibitors were present either throughout infection (black), or added at 8 hr p.i. (white).

(C) 5 mM DTT was added at given times post-addition of SV40 (solid line). Alternatively, cells were infected in the presence of 5 μM nocodazole (noc). At 2 hr p.i, noc was washed out, and 5 mM DTT was added (dashed line). DTT inhibition was similar with or without noc, a microtubule-dissociating agent that allows virus uptake into caveosomes but prevents further transport to the ER (Pelkmans et al., 2001), and thus confirmed that the DTT sensitive step occurred after exit from the caveosome.

(D) siRNA silencing was achieved by transfection of siRNAs (Figure S1). A margin for insignificant pertubations of infection (±20%) was indicated by dashed lines.

RESULTS

ER Processes Associated with SV40 Entry

We first perturbed ER-associated processes in CV-1 cells and determined 20 hr postinfection (p.i.) whether infection was affected using a FACS assay based on T-antigen expression. Inhibitors of proteasomal degradation (MG-132, omuralide), ER Ca^{2+} homeostasis (thapsigargin), and disulfide bond formation (DTT) blocked infection (Figure 1A). When added 8 hr p.i., they failed to affect infection or had only partial effects, suggesting that inhibition mainly involved early events (Figure 1B). Addition of DTT at various times after virus addition showed that the step affected occurred between 4 and 8 hr p.i. with a midpoint at 5.5 hr p.i. (Figure 1C). This correlated with the arrival of SV40 in the ER (Kartenbeck et al., 1989). Inhibition of trimming of N-linked core glycans by kifunensine (ER mannosidase inhibitor) and castanospermine (glucosidase inhibitor), or inhibition of GRP94 and other members of the heat shock protein 90 chaperones had little effect (Figure 1A).

Next, siRNA-mediated knockdown of ER proteins was performed in HeLa cells. We confirmed by immunoblotting that the level of target protein was reduced (Figures S1A–S1F in the Supplemental Data available with this article online). While no effect was observed on VSV infectivity (a virus that does not enter via the ER route, Figure S1H), depletion of two ER thiol-disulfide oxidoreductases, protein disulfide isomerase (PDI) and ERp57, significantly reduced SV40 infection (Figure 1D). In contrast, depletion of the oxidoreductase TMX3 or ERp29 (an ER protein with thioredoxin-like fold but lacking the catalytic site), and the two glycoprotein chaperones, calnexin (CNX) and calreticulin (CRT), had no effect (Figure 1D). Silencing of ERp72, another abundant ER thiol-disulfide oxidoreductase, gave divergent results for two independent siRNAs that both reduced ERp72 levels; one enhanced infection, and the other had no effect (Figure 1D).

Significant inhibition of infection was also observed after silencing of Derlin-1 and Sel1L (sel-1 suppressor of lin-like protein, Figure 1D), two transmembrane proteins involved in the export of misfolded proteins from the ER to the cytosol for proteasomal degradation (Mueller et al., 2006; Ye et al., 2004).

The results implied that ER factors involved in disulfide bond oxidation, reduction, and isomerization were critical for productive entry. In addition, calcium homeostasis and ER-associated degradation (ERAD) seemed to play a role.

Free Sulfhydryl Groups and Disulfide Bonds in Intact Virions

To pursue the oxidoreductases, we first analyzed whether disulfides and free cysteines in the virus were important for infectivity. We found that treatment of isolated virus with 5 mM DTT resulted in full reduction of all disulfide bonds in the particle (see below) but did not affect infectivity (Figure 2A) and neither did treatment with the thiol oxidant, diamide. However, alkylation using 4-acetamido-4′-maleimidylstilbene-2,2′-disulfonic acid (AMS), or iodoacetic acid (IAA), reduced infectivity by 70%–80%, suggesting that one or more free sulfhydryl groups were critical (Figure 2A). Alkylation or reduction of viruses did not affect internalization or transport to the ER, as shown by the

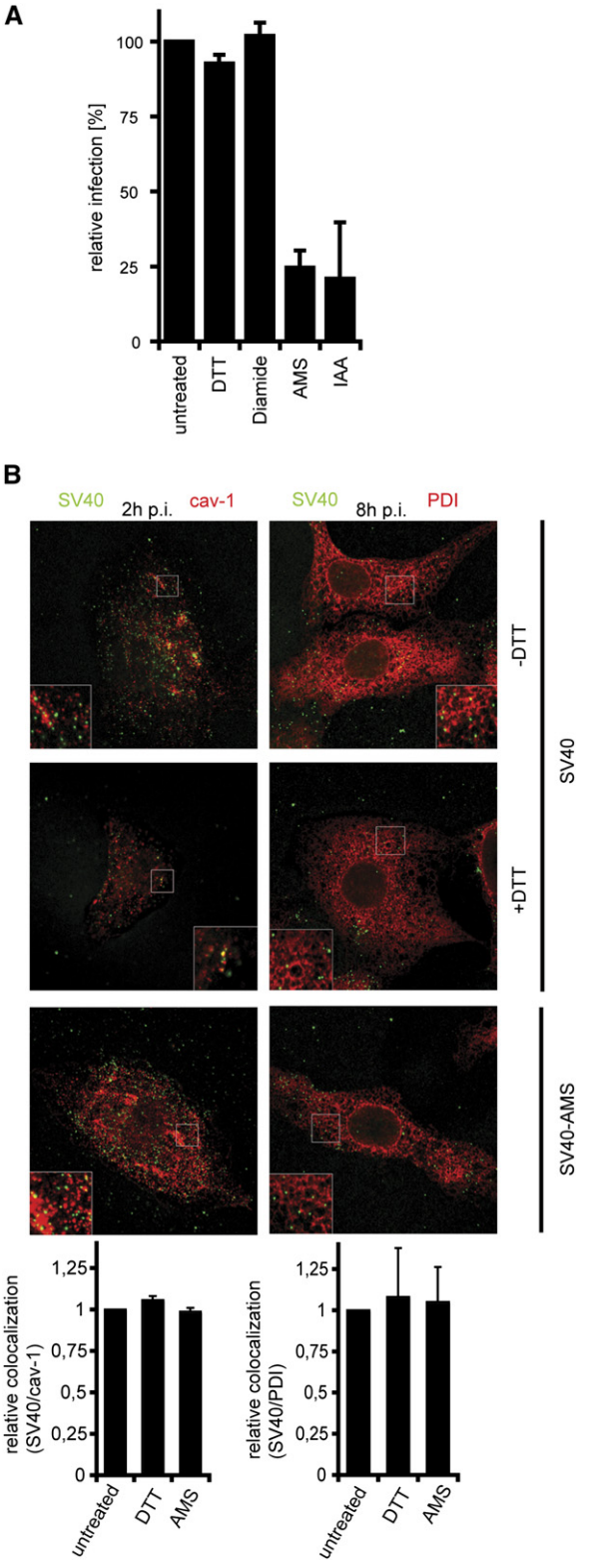

Figure 2. Free Sulfhydryls in SV40 Are Critical during Entry

CV-1 cells were infected with SV40 (1 PFU/cell [A]; 10 PFU/cell [B]). The data represent the average ± SD of three independent experiments.

colocalization of virus with caveolin-1 2 hr p.i. or with the ER marker PDI 8 hr p.i. (Figure 2B).

VP1 is the only protein in SV40 that has cysteines. The X-ray structure shows that four of the seven cysteines (C87, C207, C254, and C267) are reduced and hidden within the folded protein or in the interphase between the subunits (Figures S2A and S2B). C49 is also reduced but partially exposed on the pentamer surface (Figure S2B, arrowhead). C104 residues form interchain disulfide bonds with each other linking VP1 subunits in adjacent pentamers (Liddington et al., 1991; Stehle et al., 1996). Around the 12 pentamers located at the vertex of the icosahedral capsid, the situation is special because here the C104 from a VP1 in a five-coordinated pentamer is in close proximity to two C104 residues from VP1 in two adjacent six-coordinated pentamers (Figure S2C). The three cysteines form one disulfide while one C104 is reduced. The seventh cysteine, C9, is part of a 13-residue, N-terminal peptide that is not visible in the X-ray structure but thought to be hidden below the pentamers (Liddington et al., 1991). The inaccessibility of C9 to mercury labeling suggests that it may be disulfide bonded (Liddington et al., 1991).

To determine how many cysteines in VP1 of intact viruses were alkylated, we used a gel-shift assay based on the 5 kDa increase in the molecular weight of a protein for each cysteine alkylated by polyethylene glycol maleimide (malPEG). The observed shift indicated that only one free cysteine was accessible for alkylation, and this only in a fraction of VP1 molecules (Figure 3A, lane 2). To identify the accessible cysteine(s), we treated the virus with different alkylating agents adding distinguishable masses as outlined in Figure 3B. Subsequent mass spectrometry showed that some C104 and C49 were alkylated indicating that they were reduced and accessible in the intact virus particle (Figures 3B–3D and S3B and S3C). After DTT treatment of the virus, additional cysteines became accessible for alkylation. In addition to C104, C9 was now also alkylated indicating that in the intact virus it must be oxidized (Figures 3B–3D and S3B and S3C). Since C104 was exclusively paired with C104 and all other cysteines were reduced in the intact virus, we concluded that C9 was present in C9-C9 disulfides.

When the virus was analyzed by nonreducing SDS-PAGE after treatment with iodoacetamide (IAM) before and during exposure to SDS to alkylate free sulfhydryl groups in VP1, the majority of VP1 hardly entered the gel (Figure 3E, lane 3, arrow). We concluded that in intact viruses, the VP1 proteins were extensively crosslinked with each other through a network of C104-C104 and C9-C9 disulfide bonds. This was confirmed using sucrose velocity

(A) SV40 was thiol-disulfide modified by reduction (5 mM DTT), oxidation (5 mM diamide), or alkylation (5 mM AMS or IAA) prior to addition to cells. (B) Cells were infected with AF488 labeled SV40 in the absence or presence of 5 mM DTT. Alternatively, alkylated AF488 labeled SV40 (5 mM AMS) was added. Cells were fixed at 2 or 8 hr p.i., and immunostained for caveolin-1 or PDI, respectively. After confocal image aquisition, the amount of colocalization of SV40 (green) with cellular markers (red) was quantified and normalized to SV40 in the absence of DTT.

gradient centrifugation of alkylated and SDS-solubilized virus. The SDS-denatured viruses sedimented homogeneously as 125S particles (Figure 3F). Only a minor fraction of VP1 dissociated from these denatured particles, and was found on top of the gradient. To form such an extensive disulfide network, we surmised the C104-C104 disulfides connected adjacent pentamers as shown by the X-ray structure, whereas the C9-C9 disulfides were likely to occur both between pentamers and within pentamers.

The presence of C9-C9 and C104-C104 disulfides was confirmed by analyzing SV40 mutants in which cysteines C9 and C104 had been replaced with alanine (Ishii et al., 1994). Analysis by nonreducing SDS-PAGE showed that C9A or C104A mutants contained VP1 dimers and monomers, while C49A mutants exhibited crosslinked VP1 oligomers exactly as the wild-type (Figure 3G, lanes 1–4). The double mutant C9A/C104A was devoid of disulfide crosslinked species and contained only monomers (Figure 3G, lane 5). This confirmed our conclusion that C9-C9 and C104-C104 disulfide bonds provide the crosslinks between VP1 molecules in the particle.

Loss of Interchain Disulfide Bonds during SV40 Entry

While the network of interchain disulfide bonds contributes to the stability of extracellular virus particles, elimination of some of the bonds is probably necessary for uncoating and release of the genome during virus entry.

To determine whether interchain disulfide bonds were actually lost during infection, alkylated and nonalkylated virus particles were allowed to enter cells for different time periods up to 10 hr. The fraction of VP1 no longer crosslinked to the network of disulfides was determined by alkylating the cell lysates, treating them with SDS, and subjecting them to nonreducing SDS-PAGE. Immunoblotting showed that while the majority of interchain disulfide bonds in incoming viruses remained intact, a fraction of VP1 molecules was released from the disulfide bonded network showing up as monomers in the SDS-gel. The amount of VP1 released by SDS remained at values below 2% until 6 hr p.i., when it increased to about 20% (Figure 4A). The time course of disconnection coincided with virus arrival in the ER.

Interestingly, the alkylated viruses did not show release of monomeric VP1 during infection, suggesting that free sulfhydryl groups were needed to release VP1 molecules from the disulfide crosslinked network, a requirement consistent with a mechanism based on disulfide isomerization rather than disulfide reduction. Since the alkylated virus was non infectious, the result also implied that the loss of interchain disulfides was an essential part of the productive entry pathway.

Depletion of ERp57 by siRNA blocked the generation of decrosslinked VP1 in HeLa cells (Figure 4B). When PDI was similarly depleted, no effect was observed. This indicated that it was ERp57 that catalyzed the loss of interchain disulfides. That this occurred by disulfide isomerization rather than reduction was shown by the slightly faster migration of the released VP1 compared to the DTT reduced form of the same protein (Figure 4A, lanes 6–9). Such differences in mobility indicate presence of intrachain disulfides. Since the X-ray structure of VP1 shows no intrachain disulfides in the intact virus, one or more interchain disulfide bond(s) must have been converted by ERp57 to intrachain disulfides by isomerization.

Analysis of SV40 cysteine mutants provided additional insight into the role of disulfide bonds and ERp57. Although formation of these mutant viruses (particularly of the C104A mutant) was slower and less efficient than wild-type SV40, we could confirm that they all were infectious. As expected, siRNA-mediated depletion of ERp57 reduced infection of the C49A mutant as much as of wild-type SV40 (Figure 4C). However, ERp57 depletion did not affect infectivity of the C9A/C104A mutant, a virus lacking disulfide crosslinks between pentamers (Figure 4C). This confirmed that the role of ERp57 is, indeed, linked to the elimination of C9-C9 and/or C104-C104 interchain disulfide bonds. If such disulfides are lacking as in the C9A/C104A double mutant, ERp57 is dispensable. It is noteworthy in this context, that the C9A/C104A mutant—like the C49A mutant and the wild-type virus—was sensitive to DTT (Figure 4D). This indicated that the inhibitory effect of DTT was not due to reduction of viral disulfides, but rather to an effect on cellular factors.

ERp57 and PDI Modify SV40 Disulfides In Vitro

Incubation of isolated virus in cytosolic extracts or in a buffer mimicking the reducing and Ca^{2+}-free environment of the cytosol failed to induce loss of interchain disulfides in SV40 (Figure 5A, lanes 4 and 5, and Figure 5B). The same was found when the virus was incubated in a buffer mimicking the oxidizing conditions of the ER (Figure 5A, lane 5).

However, when either isolated PDI or ERp57 were added to the redox buffer, significant loss of interchain disulfides was observed using the SDS-PAGE assay (Figures 5D and 5E, lanes 3–6). Again, about 20% of the VP1 proteins were found to be uncoupled from the capsids using either of the oxidoreductases. When the two enzymes were inactivated by alkylation, no release of VP1 occurred indicating a direct role for the thiol-disulfide oxidoreductase function (Figures 5D and 5E, lane 7). The full effect was reached with one oxidoreductase molecule per ten viruses indicating a catalytic effect. Incubation with both oxidoreductases together did not increase the amount of monomeric VP1 (Figure 5F, lane 4).

To investigate whether ERp57 and PDI served as reductases or isomerases in vitro, alkylated SV40 was used as a substrate. PDI was found to release a similar amount of reduced VP1 as from control virus (Figure 5E, lane 8). ERp57 failed to release any VP1 (Figure 5D, lane 8). Hence, ERp57 seemed to act as an isomerase, PDI as a reductase. We also investigated whether Ca^{2+} chelation would increase the efficiency of VP1 release. Only PDI showed such an increase (Figures 5D and 5E, lane 9), suggesting that PDI acts most efficiently on disulfides when the SV40 particle has undergone a structural change induced by the loss of Ca^{2+} ions,

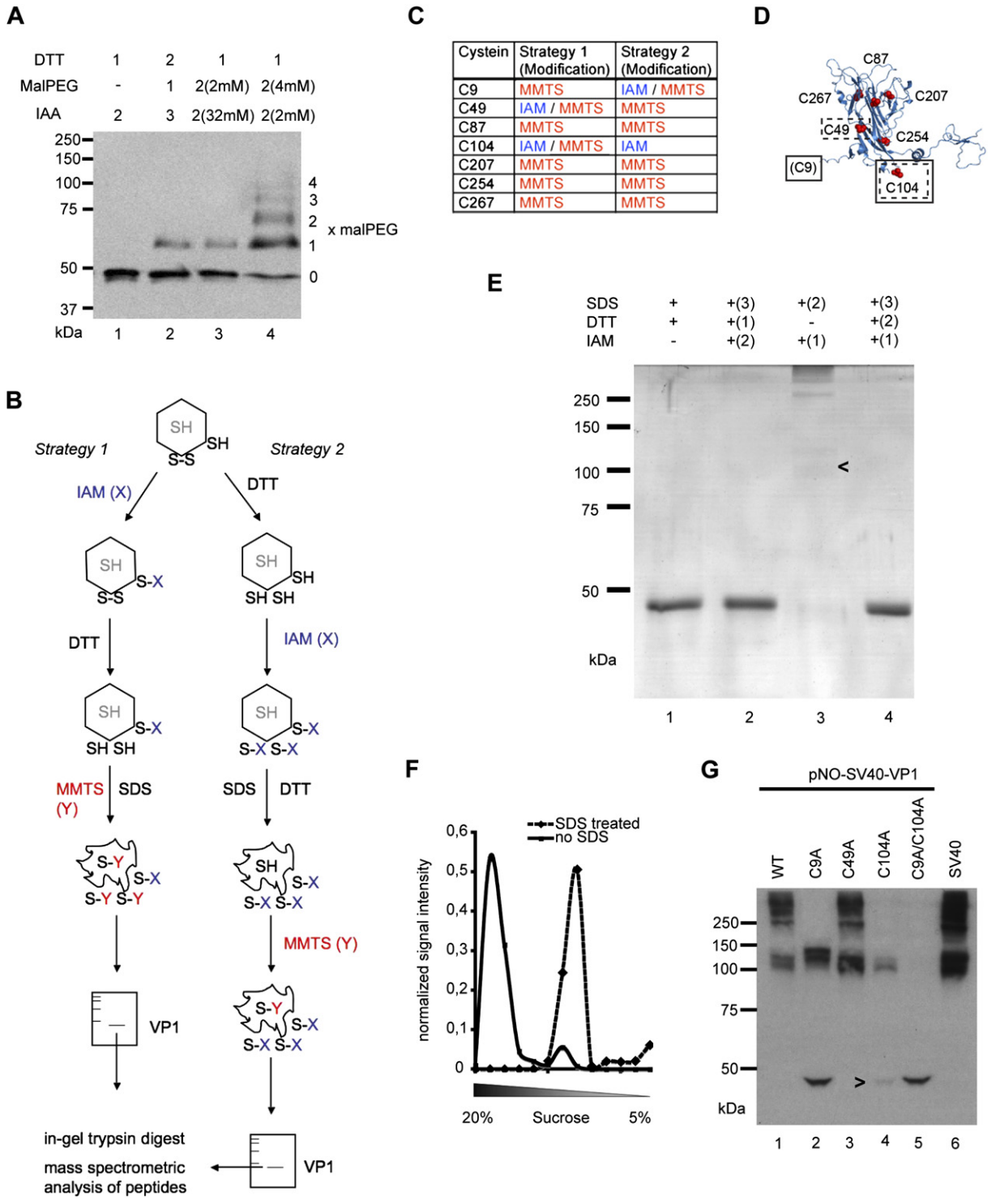

Figure 3. Characterization of SV40 Cysteines in Intact Virions

(A) Intact SV40 particles were alkylated by malPEG, followed by DTT reduction and alkylation of all remaining cysteines by IAA in the presence of SDS (lane 2). Alternatively, SV40 was reduced in the presence of SDS and alkylated with IAA (lane 1) or with malPEG/IAA mixtures (as indicated). The latter identified band shifts conferred by single or multiple (up to four) malPEG modifications (lanes 3 and 4) Numbers indicate the order of addition of the reagents.

(B) Outline for the identification of the individual SV40 cysteines present as free sulfhydryls or disulfide bonded by mass spectrometry. Strategy 1 labeled reduced and exposed cysteines differently than all other cysteines by alkylation with IAM of intact SV40. All further cysteines were alkylated

e.g., through the externalization of the C-terminal arm of VP1, which is normally held in place by the cation.

The monomeric VP1 generated in vitro after ERp57 and ERp57/PDI incubation migrated identically to VP1 released during infection in vivo (Figure 5F, compare lanes 1, 3, and 4). In contrast, the band generated by PDI alone migrated like the completely reduced species (Figure 5F, lanes 2 and 5). This was consistent with a disulfide isomerization from interchain to intrachain disulfides in VP1 by ERp57, but not by PDI.

The results showed that ERp57 eliminates interpentameric disulfide bonds in SV40. As during cell entry, ERp57 catalyzes in vitro the disconnection of about 20% of pentamers by disulfide isomerization. In contrast, PDI induces reduction of disulfides in vitro, a reaction that does not occur during virus entry.

Release of Five-Coordinated Pentamers

Judging by the mobility of VP1 in SDS gels, the stabilizing network of disulfide crosslinks was eliminated by treatment with DTT (Figure 3A, lane 2). This did not cause dissociation of the particle. Velocity centrifugation of reduced virus showed only a shift in the sedimentation coefficient from 250S for control virus to 245S (Figure 6A). A similar shift was seen when the virus was treated with the Ca^{2+}-chelating agent EGTA to remove the VP1-bound Ca^{2+} ions, and thus weakened the interpentamer connections provided by the invading C-terminal arms. Negative stain electron microscopy indicated that when applied alone, both of these treatments induced penetration of stain into the capsids, consistent with loosening pentamer contacts, but the particles remained intact (Figure 6B, b and c).

However as previously reported (Hartmann and Scott, 1981), a major structural change occurred when DTT and EGTA were added together. EM showed release of doughnut-shaped particles with a diameter of 12 nm corresponding most likely to VP1 pentamers (Figure 6B, d and e). However, amorphous capsid structures were still present with visible capsomers (Figure 6B, d).

Sucrose velocity gradient sedimentation analysis showed that combined DTT-reduction and Ca^{2+} chelation resulted in two peaks of VP1 corresponding to pentamers at the top of the gradient and modified capsids that sedimented at 230S (Figure 6A). The 230S particles contained the viral DNA but only about half of the VP1 and VP2/VP3 proteins (Figures 6C and 6D). Partial uncoating of the virus could thus be induced in vitro by combined reduction of interchain disulfide bonds and extraction of the VP1 associated Ca^{2+} ions.

When the partially uncoated viruses were viewed by cryo-electron microscopy with tomographic reconstruction, the particles had lost the capsomers located at the vertices but retained all six-coordinated capsomers (Figures 6F and S4). This suggested that the 12 five-coordinated pentamers were less tightly associated than the rest, and dissociated selectively when the interchain disulfides and the associations provided by C-terminal peptides were lost. Interestingly, when SV40 capsids devoid of DNA ("empty particles") were subjected to the same disassembly conditions, no remnant capsids were observed. The entire capsid dissociated into slowly sedimenting pentamers (Figure 6E). It is thus possible that the viral minichromosome, located in the central cavity, interacts with pentamers and increases the stability of the particle.

While no obvious structural alterations of SV40 particles incubated in vitro with ERp57 and/or PDI could be observed by EM after negative staining, sucrose velocity gradient centrifugation showed the release of 9% of pentamers after Ca^{2+} chelation (Figure 6G). This indicated that both reduction and isomerization of disulfides in vitro can lead to pentamer release. For pentamer dissociation however, the loss of disulfide bonds is not sufficient; loss of Ca^{2+} ions is also required.

Pertubation of ERAD Affects Infection

The notion that SV40 entry involves the ERAD pathway was suggested by the sensitivity of infection to proteasome inhibitors and to the silencing of Derlin-1 and Sel1L, two proteins involved in retrotranslocation (Figures 1A and 1D) (Mueller et al., 2006; Ye et al., 2004). The dependence on PDI for infection (Figure 1D) also indirectly supported such a connection because Forster et al. (2006) reported that PDI depletion causes ER retention of misfolded protein substrates. In contrast, depletion of ERp72, another abundant PDI-like protein in the ER, increases retrotranslocation of misfolded proteins (Forster et al., 2006).

by MMTS, after DTT reduction and SDS-denaturation. Strategy 2 labeled the reduced and exposed as well as the disulfide bonded cysteines differently than the reduced and hidden species (gray) by DTT reduction followed by IAM alkylation. IAM was quenched with DTT, and hidden cysteines were alkylated by MMTS in the presence of SDS. Samples were submitted to SDS-PAGE and Coomassie staining. VP1 was excised and subjected to an in-gel trypsin digest; peptides were eluted and analyzed by mass spectrometry. The mass difference for IAM and MMTS was used to distinguish individual cysteines.

(C) Summary of the thiol-modifications of VP1 cystein residues detected by mass spectrometry (see also Figure S3 and Tables S1 and S2).

(D) Ribbon diagram of a single VP1 molecule as present in a pentamer. Highlighted in red are the cysteine residues. Dashed lines indicate reduced and exposed cysteines; solid lines indicate disulfide bonded cysteines.

(E) Nonreducing SDS-PAGE and Coomassie staining of purified SV40 after treatment with SDS, DTT (lane 1), or after subsequent treatment with DTT, IAM, and SDS (lane 2), with IAM and SDS (lane 3), or with IAM, DTT, and SDS (lane 4). Numbers indicate the order of addition of reagents. All disulfides could be reduced prior to addition of SDS (lane 2). Arrowhead indicates minor amounts of dimers (lane 3).

(F) Sedimentation analysis of IAM-alkylated and SDS-denatured (as in [E], lane 3) as compared to untreated SV40 on a linear 5%–20% sucrose gradient.

(G) Wild-type and mutant SV40, where single or double cysteines had been exchanged for alanine, were produced by pNO-SV40-VP1 transfection (lanes 1–5). As control, wild-type SV40 grown by infection was used (lane 6). Preparations were alkylated (IAM), subjected to nonreducing SDS-PAGE, and immunoblotted against VP1. Arrowhead indicates monomers in the C104A mutant (lane 4).

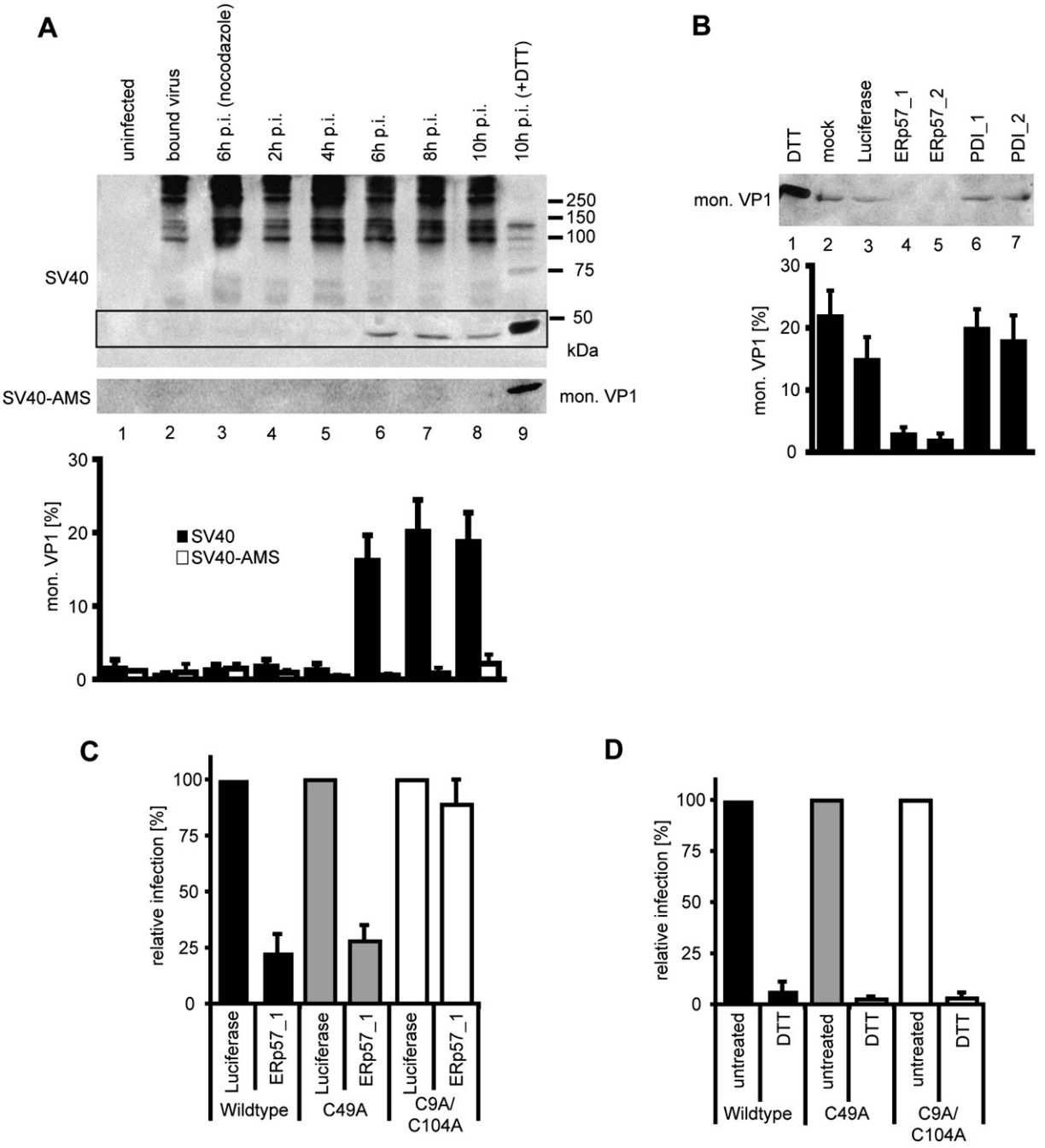

Figure 4. ERp57-Mediated Isomerization of SV40 Disulfides Decrosslinks VP1 Molecules

(A) CV-1 cells were infected with either untreated or AMS-alkylated SV40 (10 PFU/cell) for indicated times p.i. (lanes 4–9). As controls, SV40 was bound to cells at 4°C (lane 3) or infection occurred in the presence of 5 mM nocodazole (lane 2) to prevent internalization or transport from caveosomes, respectively. Cell lysates were prepared after alkylation with MMTS or NEM (data not shown). Lysates were analyzed by nonreducing SDS-PAGE and were immunoblotted against VP1. The VP1 antiserum showed much higher affinity against disulfide crosslinked molecules (especially dimers) than monomeric VP1. Hence, relative signal intensities of monomeric VP1 (boxed) were always compared to the fully reduced input (lane 9). The mean values of three independent experiments ± SD are shown.

(B) PDI and ERp57 were silenced by siRNA transfection in HeLa cells prior to infection with SV40 (50 PFU/cell). The proteins of infected cells were alkylated with 5 mM MMTS (10 hr p.i.). Cell lysates were analyzed by nonreducing SDS-PAGE and immunoblotted against VP1. Quantification as in (A).

(C) HeLa cells silenced for ERp57 were infected with mutant and wild-type SV40 (1 PFU/cell).

(D) CV-1 cells were infected with mutant and wild-type SV40 (1 PFU/cell) in the presence or absence of DTT.

The data represent the average ± SD of three independent experiments.

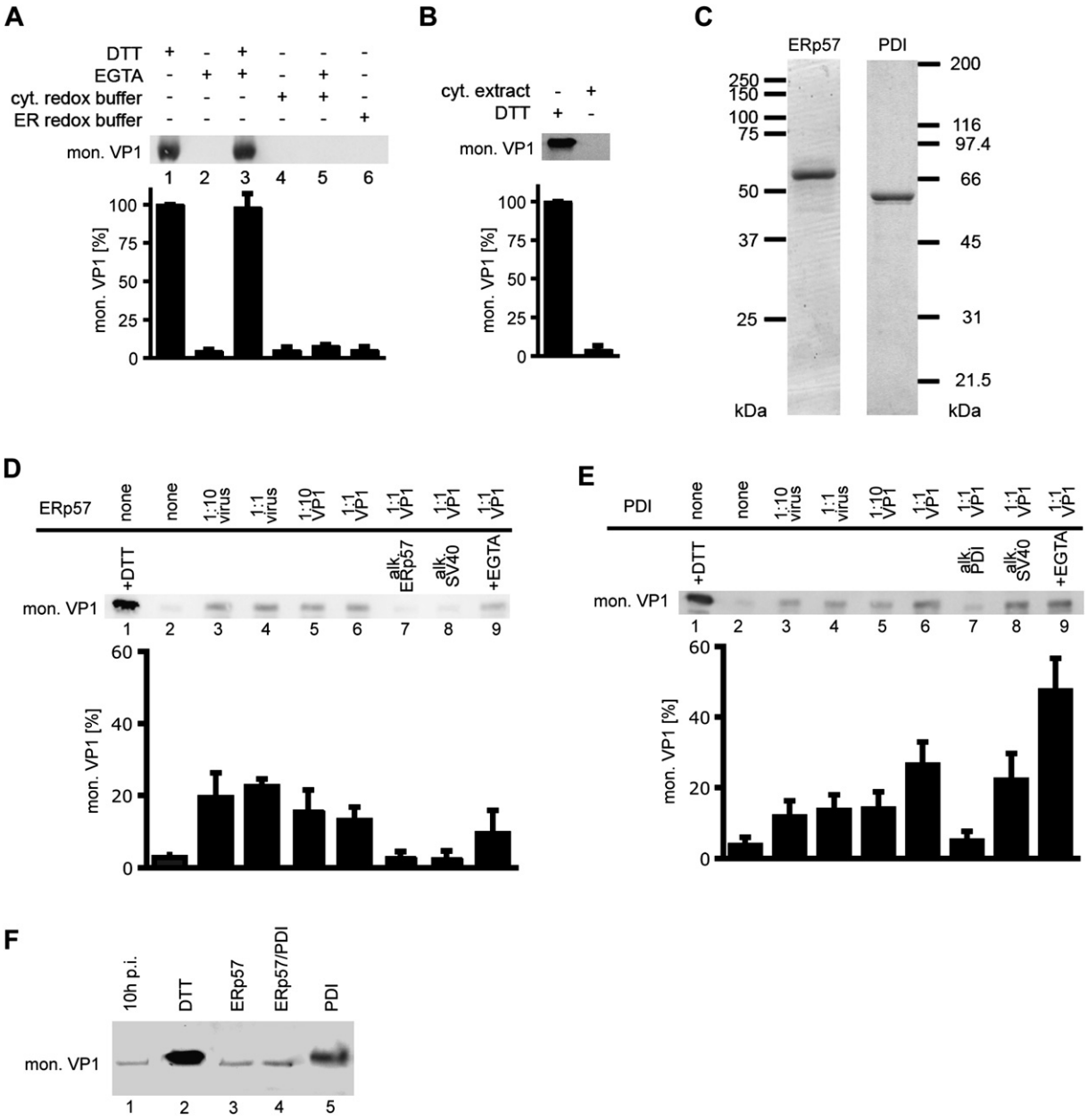

Figure 5. ERp57 Isomerizes SV40 Disulfide Bonds In Vitro

(A) SV40 was incubated for 1 hr (37°C) in glutathione redox buffer in the presence or absence of 5 mM EGTA. The molecular ratios of reduced versus oxidized glutathione (GSH:GSSG) mimicked reducing cytosolic (100:1, lanes 4 and 5) or oxidizing ER conditions (1:1, lane 6). After 5 mM IAM alkylation, nonreducing SDS-PAGE, and immunoblotting against VP1, the amount of monomeric VP1 was determined as compared to the DTT reduced input. Mean values of relative signal intensities ± SD are shown.

(B) SV40 was incubated for 1 hr (37°C) in cytosolic extracts from HeLa cells. Analysis as in (A).

(C) SDS-PAGE and Coomassie staining of purified ERp57 or PDI.

(D) 50 nM SV40 were incubated for 1 hr (37°C) in ER redox buffer in the presence or absence of 5 mM EGTA with purified ERp57 in the stoichiometries indicated. As controls, alkylated SV40 or alkylated ERp57 were used. Analysis as in (A).

(E) As in (D) using PDI instead of ERp57.

(F) Comparison of monomeric VP1 released during infection or in vitro. SV40 was treated for 1 hr (37°C) with 5 mM DTT (lane 2), ERp57 (as in [D], lane 3), PDI (as in [F], lane 5), or both thiol-disulfide oxidoreductases in equal amounts (lane 4) in vitro. Alternatively, CV-1 cells were infected for 10 hr p.i. (lane 1). Subsequently, in vitro samples or cell lysates were alkylated (5 mM MMTS), submitted to nonreducing SDS-PAGE, and immunoblotted against VP1.

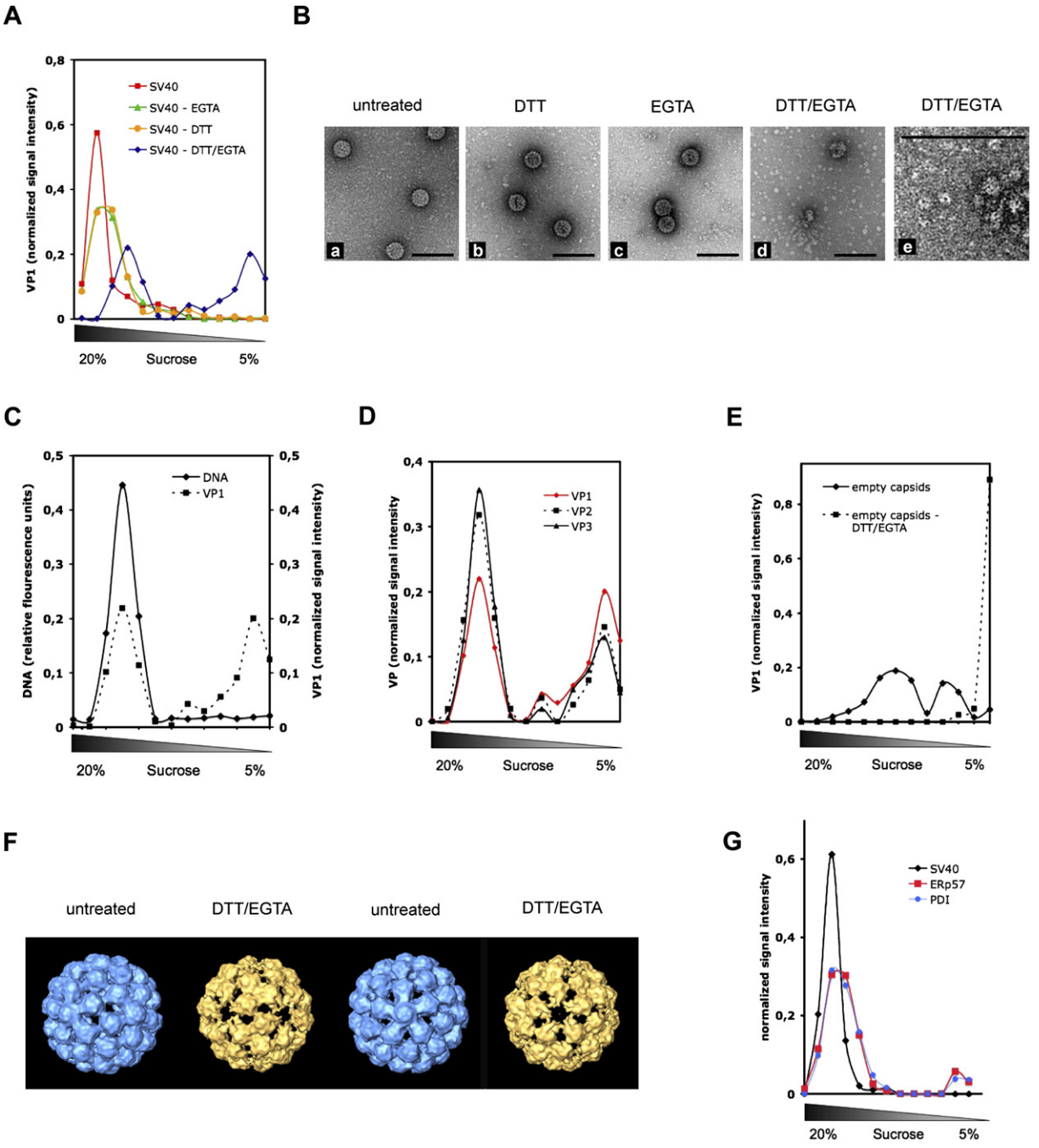

Figure 6. In Vitro Disassembly of SV40

Representative examples of three independent experiments are shown ([A–E] and [G]).

(A) Sucrose sedimentation analysis on a linear 5%–20% sucrose gradient of untreated, 5 mM DTT, 5 mM EGTA, or DTT/EGTA (5 mM/5 mM)-treated SV40. Fractions were immunoblotted against VP1.

(B) SV40 (a) was incubated with DTT (b), EGTA (c), or DTT/EGTA (d and e) as in (A), and analyzed by negative EM. Scale bars represent 100 nM.

(C) Sedimentation as in (A) after DTT/EGTA incubation of SV40. To determine the viral DNA, samples were phenol/chloroform extracted, and DNA was EtOH precipitated and quantified.

(D) As in (A). Fractions immunoblotted against VP1 and VP2/VP3.

(E) As in (A). Instead of infectious SV40, so-called empty particles lacking the minichromosome were used.

(F) Surface rendering of the three-dimensional structure of SV40 from cryo-electron tomography after icosahedral symmetrization without (blue) or with (yellow) preincubation with DTT/EGTA. Left structure pair shows the typical orientation of the capsomers, the right structure pair is rotated horizontally to allow the view onto a vertex, revealing the missing vertex in the DTT/EGTA-treated SV40. Control virus represents average of multiple

To pursue the issue further, we tested whether the cysteine mutants C49A and C9A/C104A were also dependent on these factors. Infectivity of mutant and wild-type SV40 was similarly sensitive to proteasome inhibitors, and to PDI and Derlin-1 depletion (Figures 7A and 7B). The sensitivity of the C9A/C104A mutant showed that the step affected by these perturbations was independent of the ERp57-mediated disulfide isomerization step.

To confirm that retrotranslocation was affected by these perturbations, we measured the level of polyubiquitinated proteins in cells using SDS-PAGE combined with immunoblotting for polyubiquitin tagged proteins (Figure 7C). We found as expected that incubation with the proteasome inhibitor MG-132 resulted in accumulation of polyubiquitinated proteins. However, when Derlin-1 or Sel1L were depleted by siRNAs and MG-132 added, fewer polyubiquitinated proteins accumulated compared to control cells, suggesting that misfolded proteins failed to exit the ER and thus, failed to be ubiquitinated (Figure 7D). Depletion of ERp57 by siRNAs had no effect while the depletion of PDI by siRNAs resulted in a clear reduction in the level of polyubiquitinated protein in the presence of MG-132 (Figure 7D). In ERp72 depleted cells, the situation was less clear. An increase was seen for the same siRNA that also dramatically enhanced SV40 infectivity (Figure 7D). We concluded that when PDI levels were reduced, and retrotranslocation was impaired, SV40 infectivity was suppressed, while ERp72 depletion, which had the opposite effect on retrotranslocation of proteins, seemed to enhance SV40 infectivity. Together with the effects of Derlin-1 and Sel1L silencing, these results were consistent with a role for ER retrotranslocation in SV40 entry.

DISCUSSION

Our results indicated that SV40 has chosen the ER route of entry so that it can take advantage of the protein folding and quality control machinery in the ER for initial uncoating and membrane translocation. Through an ERp57-catalyzed disulfide isomerization reaction in the ER lumen, a sub-population of pentamers (most likely the 12 vertex pentamers) are disconnected from an extensive network of disulfide crosslinked VP1 molecules in the capsid, the first step in the uncoating of SV40. The dependence on Derlin-1, Sel1L, and PDI suggested that the modified virus makes use of the ERAD pathway presumably for transport into the cytosol. We hypothesize that the vertex pentamers are lost when the virus reaches the low Ca^{2+} in the cytosol. The overall strategy used by SV40 is thus similar to that previously described for cholera toxin but more elaborate due to the structural complexity of the particle (Tsai et al., 2001).

We found that the SV40 capsid is extensively crosslinked by interpentameric and possibly also intrapentameric C104-C104 and C9-C9 disulfide bonds between VP1 molecules. The C9-C9 bonds are not visible in the X-ray structure because the terminal residues of the N-terminus are disordered (Liddington et al., 1991). Through these bonds, virtually all VP1 molecules in the particle are covalently connected with each other.

The main function of the disulfide bond network is most likely to stabilize the virus during extracellular passage. Although the virus remains intact after reduction of all disulfides, it is less stable particularly in a low calcium environment. Mutations in C9, C104, or both have been shown to result in formation of unstable particles that possess reduced infectivity (Gharakhanian et al., 2001).

Of the VP1 cysteines, C9, C104, and C257 are conserved among polyoma viruses. Interestingly, an extended disulfide bonded network is not present in mouse polyoma virus. The X-ray structure shows the presence of C19-C114 intrachain disulfides. In SV40, these correspond to C9-C104 disulfides. Although polyoma virus also enters the ER, recent studies suggest that the uncoating mechanisms may be different (Lilley et al., 2006; Magnuson et al., 2005).

A covalently crosslinked capsid shell obviously necessitates special measures during entry. To allow opening of the capsid and release of the viral chromosome, at least some of the crosslinks must be eliminated. We found that about 20% of the VP1 molecules were in fact uncoupled from an otherwise intact network of disulfide-bonded VP1s. Since the VP1 s in the mature particle contain no intrachain disulfide bonds, such bonds in the disconnected VP1s likely resulted from an isomerization reaction in which an interchain disulfide was isomerized to an intrachain disulfide. When the acceptor cysteines were alkylated, no isomerization was possible, no VP1 molecules were released, and the virus was noninfectious. When SV40 was incubated in a cytosolic extract or in glutathione redox buffers mimicking conditions in the ER or cytosol, there was no reduction or isomerization of disulfides, consistent with the need for a thiol-disulfide oxidoreductase in the isomerization process.

The evidence that ERp57 was the thiol-disulfide oxidoreductase required was four-fold. First, siRNA silencing of this abundant, soluble ER enzyme resulted in a 5-fold reduction of SV40 infection. Second, with ERp57 silenced, VP1 disconnection from the disulfide crosslinked network did not occur. Third, incubation of SV40 in vitro with isolated ERp57 reproduced in every detail the observations made in vivo. Finally, infection by the C9A/C104A mutant that lacks disulfide bonds was not sensitive to ERp57 silencing.

viruses; while due to the overall heterogeneity in virus diameter in the DTT/EGTA-treated population, the structure shown is from one capsid to allow a clearer view for the hexameric capsomers. The missing vertex density was, despite the heterogeneity in this preparation, the striking feature of the structure averaged from all reconstructed DTT/EGTA-treated capsids.

(G) Sedimentation of SV40 after incubation with ERp57 or PDI, and EGTA addition (as in Figures 5D and 5E, lane 9) on a linear 5%–20% sucrose gradient. Fractions were immunoblotted against VP1. EGTA addition was essential for pentamer release.

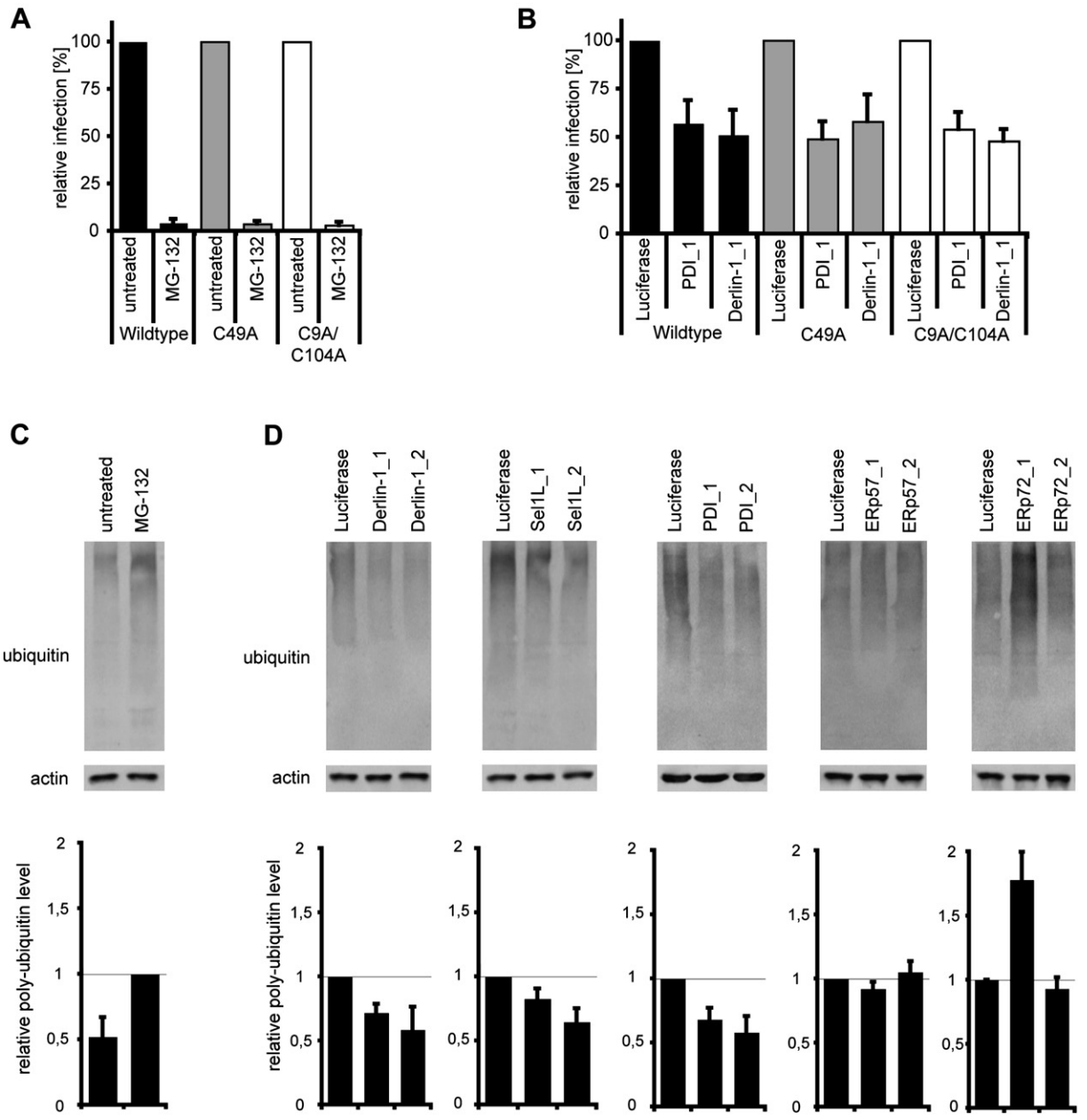

Figure 7. Interference with ER to Cytosole Retrotranslocation Coincides with Pertubation of SV40 Infection

(A) CV-1 cells were infected with SV40 (wild-type and cysteine mutants) in the presence or absence of the proteasome inhibitor MG-132 (20 μM). The data represent the average ± SD of three independent experiments.

(B) HeLa cells that were silenced with siRNAs directed against Derlin-1, PDI, or Luciferase were infected with SV40 (wild-type and cysteine mutants). The data represent the average ± SD of three independent experiments.

(C) HeLa cells were treated with MG-132 for 16 hr. Cell lysates were subjected to SDS-PAGE and immunoblotted against ubiquitin. Shown are the polyubiquitinated proteins (poly-Ub). Poly-Ub levels as compared to MG-132-treated cells were depicted as mean ± SD.

(D) Poly-Ub levels under siRNA-silencing conditions: HeLa cells were silenced for Derlin-1, Sel1L, PDI, ERp57, or ERp72, and all cells were treated for16 hr with MG-132 prior to cell lysis. Poly-UB levels as compared to control cells (Luciferase) were depicted as mean ± SD.

Our results suggested that ERp57 reduces a C9-C9 disulfide and replaces it with the C9-C104 intrachain disulfide by using the free C104 in the threesome of cysteines at the vertex as acceptor. The corresponding C19-C114 disulfide of mouse polyomavirus indicated the feasibility of this connection (Stehle et al., 1996). It is noteworthy, that only at the vertex, a cluster of three closely spaced C104 residues involving one VP1 of a five-coordinated pentamer and two VP1s in neighboring six-coordinated pentamers exists (Stehle et al., 1996; Figure S2). The

weak electron density in this region could be explained by flexibility and/or by randomness as to which of the cysteines participate in the C104-C104 disulfide bond (Stehle et al., 1996). With two of the C104 cysteines disulfide bonded, one must remain reduced. Our results indicated that this free sulfhydryl was essential in the initial uncoating process; when it was alkylated the virus reached the ER but failed to infect. The second cysteine residue accessible for alkylation, C49, is located too far from the disulfides to serve as an acceptor for isomerization, and the properties of the C49A mutant virus did not differ from the wild-type.

As a consequence of the loss of the C9-C9 disulfide, the covalent connections between the vertex pentamers and the hexavalent neighbors are lost. Although 20% of the VP1 molecules no longer participate in the disulfide-bonded network, all pentamers remain associated with the virus particle as long as the Ca^{2+} ions are in place. Our in vitro experiments using cryo-electron tomography and mass spectrometry suggested that the pentamers disconnected from the crosslinked network constitute the 12 vertex pentamers. At least in vitro, we found that the release of these pentamers from a reduced particle required extraction of the Ca^{2+} ions known to stabilize the interaction between VP1 and the C-terminal arm of a neighboring VP1. Thus, to release the vertex pentamers, both the covalent disulfide connections had to be broken and the C-terminal arms had to dissociate from the neighboring pentamers.

Although clearly favored by our observations, a role for ERp57 in SV40 uncoating raised some questions. How can this enzyme reach cysteines and disulfide bonds located on the inner surface of the capsid wall? The dimensions of ERp57 can be deduced from the crystal structure of the b-b′ domain and analytical ultracentrifugation studies; the thioredoxin-like domains have a diameter of about 3.5 nm (Frickel et al., 2004; Kozlov et al., 2006). The X-ray structure of the virus shows that the capsid wall has openings of about 3-5 nm in size (Liddington et al., 1991), which may be big enough if one considers the dynamics of viral capsids, i.e., so-called "breathing" (Lewis et al., 1998), and if one assumes a flexible structure for the oxidoreductase (Tian et al., 2006).

Another question concerns the association of ERp57 with calnexin (CNX) and calreticulin (CRT), and its function as a thiol-disulfide oxidoreductase for glycoproteins. We did not observe any effect on infectivity by inhibitors that block glycoprotein trimming and entry into the CNX/CRT cycle. siRNA silencing of CNX and CRT failed to affect virus infection. It is therefore likely that ERp57 interacts with SV40 independently of CNX and CRT.

While essential for productive entry of the wild-type virus, we found that ERp57 was dispensable for the C9A/C104A mutant, a virus devoid of disulfide bonds. That this mutant virus was still sensitive to DTT, to proteasome inhibitors, and to the depletion of Derlin-1, Sel1L, and PDI indicated that there are ER-associated steps during entry beyond ERp57-induced rearrangement of disulfide bonds. That these events included translocation of the virus from the ER lumen to the cytosol was suggested by the identity of the factors and inhibitors identified. Derlin-1 is a membrane protein involved in the translocation of ERAD substrates from the ER to the cytosol for degradation by proteasomes (Ye et al., 2004). Sel1L is predicted to be a type I transmembrane protein and thought to function in substrate recognition for ERAD (Mueller et al., 2006). PDI silencing has been shown to inhibit polyubiquitination of proteins and retrotranslocation of misfolded proteins (Forster et al., 2006; Tsai et al., 2002), and proteasome inhibitors can impair retrograde transport of ERAD substrates (Hirsch and Ploegh, 2000). Finally depletion of ERp72, another abundant thiol-disulfide oxidoreductase, by an siRNA that enhanced retrotranslocation of ERAD substrates (Figure 7B)(Forster et al., 2006), also enhanced SV40 infection.

These observations indicate that SV40 exploits a machinery in the ER normally reserved for identification of misfolded proteins and for retrotranslocation of these proteins through the ER membrane. The ER is the only organelle in the cell that possesses a retrotranslocation system for macromolecules, a system known to be exploited by certain bacterial toxins and possibly other viruses (Lilley et al., 2006; Tsai et al., 2002). How this interaction works for SV40 at the molecular level poses an interesting problem given the large size of the virus particles. Future work will have to obtain direct evidence on how the translocation of the virus from the ER to the cytosol is achieved.

The overall process is likely to involve additional changes in the virus such as exposure of VP2/VP3 either in the ER lumen or after translocation (Daniels et al., 2006; Norkin et al., 2002), and the exposure of nuclear localization signals required for import into the nucleus (Clever et al., 1991; Nakanishi et al., 1996). Although we have shown here that uncoating starts in the ER by the isomerization of disulfide bonds, we find it likely that pentamers dissociate from the particle in the cytosol when the virus encounters a milieu with a low Ca^{2+} concentration. The inhibitory effect of thapsigargin may be explained by the elevation in Ca^{2+} in the cytosol (Scharff et al., 1988). The stepwise uncoating program of SV40, which we partially unraveled in this study, clearly provides many interesting questions for future investigation.

EXPERIMENTAL PROCEDURES

Cells, Viruses, Antibodies, and Materials

CV-1 and HeLa cells were from ATCC. SV40 was grown in CV-1 cells, purified, and flourescently labeled as described (Pelkmans et al., 2001). Mutant SV40 and recombinant VSV expressing GFP were prepared as described (Ishii et al., 1994; Pelkmans and Zerial, 2005). Antibodies were from StressGene (PDI, SPA890; ERp72, SPS720), Santa Cruz Biotechnology (caveolin-1, Cav1N2), Alexis Biochemicals (Sel1L, MSel1), or Sigma (beta-actin, AC-15; ubiquitin, U5379). Antibodies against T-antigen (T-ag), VP1, ERp29, TMX3, and ERp57 have been described (Frickel et al., 2004; Haugstetter et al., 2005; Pelkmans et al., 2001, 2002; Rainey-Barger et al.,

2007). VP2/3 antiserum was raised in rabbits immunized with the synthetic C-terminal VP2/3 peptide (CSASAKARHKRRNRSSRS). Secondary antibodies and AMS were from Molecular Probes. Methyl methanethiosulfonate (MMTS) and N-ethylmaleimide (NEM) from Pierce, malPEG from Eprova, MG-132 and thapsigargin from Calbiochem, omuralide from Cayman Chemicals, kifunensine from Toronto Research Chemicals, and geldanamycin from AG Scientific. All other reagents were from Sigma.

Infection Studies

Cells were infected with SV40. At 20 hr p.i., cells were trypsinized, fixed in 4% formaldehyde, permeabilized with 0.05% saponin, and incubated in FACS buffer (20 mM EDTA, 0.02% NaN_3, 2% FCS, 0.1% saponin, PBS pH 7.4) successively with α-T-ag and α-mouse AF647 antibodies. Cells were analyzed for T-ag signals by FACS. 10,000 cells were counted, and the percentage of cells with T-ag signal (infected cells, ≈20%) was determined and normalized to 100% for the control situation. In each case, mean values of minimum three independent experiments ± standard deviation (SD) were shown.

siRNA-Mediated Silencing

siRNA experiments were performed with siRNAs from QIAGEN or Ambion (Figure S1). Silencing was achieved by double transfection of 10^5 HeLa cells with Hiperfect (QIAGEN). 48–72 hr posttransfection (Figure S1) cells were infected with SV40, or cell lysates were prepared.

Thiol-Disulfide Modification of SV40

Thiol-disulfide modifications were performed successively for 1 hr (RT) in the dark by addition of reagents in virion buffer (10 mM HEPES [pH 8.0], 150 mM NaCl, and 1 mM $CaCl_2$). For in vitro disassembly, virus was incubated with 5 mM dithiothreitol (DTT), 5 mM EGTA, or both. Alternatively, virus was dialyzed O.N. (4°C) against glutathione redox buffer, or added to cytosolic extracts of HeLa cells (Kutay et al., 1997) which contained 8 mM reduced glutathione. For sequential alkylation of reduced and oxidized cysteines, initially 5 mM alkylating reagent was added, followed by subsequent addition of 10 mM DTT and 20 mM alkylating reagent different to the one initially used as indicated. 2% SDS was present during the final alkylation reaction, if indicated.

Immunofluorescence Microscopy

CV-1 cells were seeded on glass coverslips and incubated with AF488-labeled SV40 for 2 hr. At 2 or 8 hr p.i., cells were fixed in 2% formaldehyde, permeabilized with 0.05% saponin, and incubated with the appropiate primary and secondary antibodies. Cells were analyzed by confocal microscopy (Zeiss 510 meta). Signals were obtained within a linear range of intensities. The amount of signal overlap was quantified for each confocal slice using Zeiss software. The signal overlap (30%–70%) was determined for at least ten fields of view per experiment and all confocal slices thereof. The signal overlap was normalized to 1 for unperturbed SV40 and compared to SV40 in the presence of 5 mM DTT, or to AMS-alkylated SV40.

Biochemical Analysis of SV40 during Infection

The proteins of infected cells were alkylated by incubation with either NEM or MMTS (5 mM) for 15 min at 37°C in the dark, lysates were prepared followed by nonreducing SDS-PAGE and immunoblotting.

In Vitro Analysis of ERp57- and PDI-Mediated SV40 Disulfide Modifications

ERp57 and PDI were purified as described (Frickel et al., 2004). SV40, ERp57, and PDI were dialyzed O.N. (4°C) against glutathione redox buffers (virion buffer including reduced (GSH) and oxidized (GSSG) glutathione: for cytosolic conditions 8 mM GSH, 80 nM GSSG, for ER conditions 4 mM GSH, 4 mM GSSG). 50 nM SV40 and indicated amounts of ERp57 or PDI were mixed and incubated at 37°C for 1 hr. Samples were alkylated (5 mM IAM), and analyzed by nonreducing SDS-PAGE and immunoblotting.

Sucrose Gradient Sedimentation

Samples were loaded on 5%–20% linear sucrose gradients (10 mM HEPES pH 8.0, 50 mM NaCl), and centrifuged for 75 min at 220,000 g (4°C). Fractions were TCA-precipitated and analyzed for VP1 or VP2/3 content by SDS-PAGE and immunoblotting. Signal intensities were recorded using a Storm scanning device within linear range and densitrometrically analyzed using ImageJ (NIH). Alternatively, phenol-chloroform extracted fractions were analyzed for dsDNA content by the Quant-It DNA assay kit (Molecular Probes). In each case, normalized signal intensities for a representative gradient of minimum three independent experiments are given.

Electron Microscopy

Virus samples were applied on a carbon-coated 400-mesh for 30 s. Grids were stained for 30 s with 2% (w/v) uranyl acetate in ddH2O. Transmission electron microscopy was performed using a FEI Morgagni 268D electron microscope at 100 kV. Images were analyzed using Soft Imaging System Software (analySIS).

Supplemental Data

Supplemental Data include Supplemental Experimental Procedures, Supplemental References, four figures, and two Excel tables and can be found with this article online at http://www.cell.com/cgi/content/full/131/3/516/DC1/.

ACKNOWLEDGMENTS

We thank Drs. J. Kartenbeck and R. Mancini for help with electron microscopy, U. Kutay for cytosolic HeLa cell extracts, S. Mkrtchian for ERp29 antibodies, and H. Kasamatsu for SV40 cysteine mutant plasmids. This work was supported by the Deutsche Forschungsgemeinschaft to M.S. and K.G., Swiss National Science Foundation to A.H. and L.P., the European Science Foundation to L.P., ETH Zurich to J.H. and A.H., the Novo Nordisk Foundation to L.E., and by the Swedish society for medical research (SSMF) to J.M.

Received: March 28, 2007
Revised: August 1, 2007
Accepted: September 28, 2007
Published: November 1, 2007

REFERENCES

Clever, J., Yamada, M., and Kasamatsu, H. (1991). Import of simian virus 40 virions through nuclear pore complexes. Proc. Natl. Acad. Sci. USA *88*, 7333–7337.

Damm, E.M., Pelkmans, L., Kartenbeck, J., Mezzacasa, A., Kurzchalia, T., and Helenius, A. (2005). Clathrin- and caveolin-1-independent endocytosis: entry of simian virus 40 into cells devoid of caveolae. J. Cell Biol. *168*, 477–488.

Daniels, R., Rusan, N.M., Wadsworth, P., and Hebert, D.N. (2006). SV40 VP2 and VP3 insertion into ER membranes is controlled by the capsid protein VP1: implications for DNA translocation out of the ER. Mol. Cell *24*, 955–966.

Estes, M.K., Huang, E.S., and Pagano, J.S. (1971). Structural polypeptides of simian virus 40. J. Virol. *7*, 635–641.

Forster, M.L., Sivick, K., Park, Y.N., Arvan, P., Lencer, W.I., and Tsai, B. (2006). Protein disulfide isomerase-like proteins play opposing roles during retrotranslocation. J. Cell Biol. *173*, 853–859.

Frickel, E.M., Frei, P., Bouvier, M., Stafford, W.F., Helenius, A., Glockshuber, R., and Ellgaard, L. (2004). ERp57 Is a Multifunctional Thiol-Disulfide Oxidoreductase. J. Biol. Chem. *279*, 18277–18287.

Gharakhanian, E., Fasching, C.L., Orlando, S.J., and Perez, A.R. (2001). Cys(9), Cys(104) and Cys(207) of simian virus 40 Vp1 are essential for infectious virion formation in CV-1 cells. J. Gen. Virol. *82*, 1935–1939.

Hartmann, J.P., and Scott, W.A. (1981). Distribution of DNase I-sensitive sites in simian virus 40 nucleoprotein complexes from disrupted virus particles. J. Virol. *37*, 908–915.

Haugstetter, J., Blicher, T., and Ellgaard, L. (2005). Identification and characterization of a novel thioredoxin-related transmembrane protein of the endoplasmic reticulum. J. Biol. Chem. *280*, 8371–8380.

Hirsch, C., and Ploegh, H.L. (2000). Intracellular targeting of the proteasome. Trends Cell Biol. *10*, 268–272.

Ishii, N., Nakanishi, A., Yamada, M., Macalalad, M.H., and Kasamatsu, H. (1994). Functional complementation of nuclear targeting-defective mutants of simian virus 40 structural proteins. J. Virol. *68*, 8209–8216.

Kartenbeck, J., Stukenbrok, H., and Helenius, A. (1989). Endocytosis of simian virus 40 into the endoplasmic reticulum. J. Cell Biol. *109*, 2721–2729.

Kozlov, G., Maattanen, P., Schrag, J.D., Pollock, S., Cygler, M., Nagar, B., Thomas, D.Y., and Gehring, K. (2006). Crystal structure of the bb' domains of the protein disulfide isomerase ERp57. Structure *14*, 1331–1339.

Kutay, U., Bischoff, F.R., Kostka, S., Kraft, R., and Gorlich, D. (1997). Export of importin alpha from the nucleus is mediated by a specific nuclear transport factor. Cell *90*, 1061–1071.

Lewis, J.K., Bothner, B., Smith, T.J., and Siuzdak, G. (1998). Antiviral agent blocks breathing of the common cold virus. Proc. Natl. Acad. Sci. USA *95*, 6774–6778.

Li, P.P., Naknanishi, A., Tran, M.A., Ishizu, K., Kawano, M., Phillips, M., Handa, H., Liddington, R.C., and Kasamatsu, H. (2003). Importance of Vp1 calcium-binding residues in assembly, cell entry, and nuclear entry of simian virus 40. J. Virol. *77*, 7527–7538.

Liddington, R.C., Yan, Y., Moulai, J., Sahli, R., Benjamin, T.L., and Harrison, S.C. (1991). Structure of Simian virus 40 at 3.8-Å resolution. Nature *354*, 278–284.

Lilley, B.N., Gilbert, J.M., Ploegh, H.L., and Benjamin, T.L. (2006). Murine polyomavirus requires the endoplasmic reticulum protein Derlin-2 to initiate infection. J. Virol. *80*, 8739–8744.

Magnuson, B., Rainey, E.K., Benjamin, T., Baryshev, M., Mkrtchian, S., and Tsai, B. (2005). ERp29 Triggers a Conformational Change in Polyomavirus to Stimulate Membrane Binding. Mol. Cell *20*, 289–300.

Marsh, M., and Helenius, A. (2006). Virus entry: open sesame. Cell *124*, 729–740.

Mueller, B., Lilley, B.N., and Ploegh, H.L. (2006). SEL1L, the homologue of yeast Hrd3p, is involved in protein dislocation from the mammalian ER. J. Cell Biol. *175*, 261–270.

Nakanishi, A., Clever, J., Yamada, M., Li, P.P., and Kasamatsu, H. (1996). Association with capsid proteins promotes nuclear targeting of simian virus 40 DNA. Proc. Natl. Acad. Sci. USA *93*, 96–100.

Norkin, L.C., Anderson, H.A., Wolfrom, S.A., and Oppenheim, A. (2002). Caveolar endocytosis of simian virus 40 is followed by brefeldin A-sensitive transport to the endoplasmic reticulum, where the virus disassembles. J. Virol. *76*, 5156–5166.

Pelkmans, L., Kartenbeck, J., and Helenius, A. (2001). Caveolar endocytosis of simian virus 40 reveals a new two-step vesicular-transport pathway to the ER. Nat. Cell Biol. *3*, 473–483.

Pelkmans, L., Puntener, D., and Helenius, A. (2002). Local Actin Polymerization and Dynamin Recruitment in SV40-Induced Internalization of Caveolae. Science *296*, 535–539.

Pelkmans, L., and Zerial, M. (2005). Kinase-regulated quantal assemblies and kiss-and-run recycling of caveolae. Nature *436*, 128–133.

Rainey-Barger, E.K., Mkrtchian, S., and Tsai, B. (2007). Dimerization of ERp29, a PDI-like protein, is essential for its diverse functions. Mol. Biol. Cell *18*, 1253–1260.

Scharff, O., Foder, B., Thastrup, O., Hofmann, B., Moller, J., Ryder, L.P., Jacobsen, K.D., Langhoff, E., Dickmeiss, E., Christensen, S.B., et al. (1988). Effect of thapsigargin on cytoplasmic Ca2+ and proliferation of human lymphocytes in relation to AIDS. Biochim. Biophys. Acta *972*, 257–264.

Stehle, T., Gamblin, S.J., Yan, Y., and Harrison, S.C. (1996). The structure of simian virus 40 refined at 3.1 A resolution. Structure *4*, 165–182.

Tian, G., Xiang, S., Noiva, R., Lennarz, W.J., and Schindelin, H. (2006). The crystal structure of yeast protein disulfide isomerase suggests cooperativity between its active sites. Cell *124*, 61–73.

Tsai, B., Gilbert, J.M., Stehle, T., Lencer, W., Benjamin, T.L., and Rapoport, T.A. (2003). Gangliosides are receptors for murine polyoma virus and SV40. EMBO J. *22*, 4346–4355.

Tsai, B., Rodighiero, C., Lencer, W.I., and Rapoport, T.A. (2001). Protein disulfide isomerase acts as a redox-dependent chaperone to unfold cholera toxin. Cell *104*, 937–948.

Tsai, B., Ye, Y., and Rapoport, T.A. (2002). Retro-translocation of proteins from the endoplasmic reticulum into the cytosol. Nat. Rev. Mol. Cell Biol. *3*, 246–255.

Varshavsky, A.J., Nedospasov, S.A., Schmatchenko, V.V., Bakayev, V.V., Chumackov, P.M., and Georgiev, G.P. (1977). Compact form of SV40 viral minichromosome is resistant to nuclease: possible implications for chromatin structure. Nucleic Acids Res. *4*, 3303–3325.

Ye, Y., Shibata, Y., Yun, C., Ron, D., and Rapoport, T.A. (2004). A membrane protein complex mediates retro-translocation from the ER lumen into the cytosol. Nature *429*, 841–847.